Carbohydrate Polymers 114 (2014) 384–391

Contents lists available at ScienceDirect

Carbohydrate Polymers

journal homepage: www.elsevier.com/locate/carbpol

Structural and conformational study of the O-polysaccharide produced by the metabolically versatile photosynthetic bacterium *Rhodopseudomonas palustris* strain BisA53

Alba Silipo[a,*], Flaviana Di Lorenzo[a], Antonia De Felice[a], Adele Vanacore[a], Cristina De Castro[a], Djamel Gully[b], Rosa Lanzetta[a], Michelangelo Parrilli[a], Eric Giraud[b], Antonio Molinaro[a]

[a] *Dipartimento di Scienze Chimiche, Complesso Universitario Monte Sant'Angelo, Università di Napoli Federico II, Via Cintia 4, I-80126 Napoli, Italy*
[b] *IRD, Laboratoire des Symbioses Tropicales et Méditerranéennes (LSTM), UMR IRD/SupAgro/INRA/UM2/CIRAD, TA-A82/J – Campus de Baillarguet, 34398 Montpellier Cedex 5, France*

ARTICLE INFO

Article history:
Received 22 July 2014
Received in revised form 18 August 2014
Accepted 19 August 2014
Available online 27 August 2014

Keywords:
Rhodopseudomonas palustris
Lipopolysaccharide
C-branched sugar
NMR spectroscopy
Molecular modeling

ABSTRACT

Rhodopseudomonas palustris is a purple photosynthetic bacterium characterized by a versatile nature and a remarkable ability to adapt to various environments. In this work, we focused our attention to its membrane characteristics and defined the structural and conformational features of the O-chain polysaccharide of LPS isolated from *R. palustris* strain BisA53. This strain produces a polymer with a trisaccharide repeating unit characterized by D-rhamnose, 3-deoxy-D-*lyxo*-2-heptulosaric acid (Dha), and a novel C-branched monosaccharide, a 4-amino-4,6-dideoxy-3-C-methyl-2-O-methyl-α-L-glucopyranose whose absolute configuration has been determined by a combination of 2D NMR spectroscopy and molecular mechanic and dynamic simulation.

1. Introduction

Rhodopseudomonas palustris is a purple photosynthetic bacterium that has been found able to dwells both in soil and water. Actually, it develops the ability to sense and adapt to environmental changes and can grow in a wide variety of habitats and conditions like swine waste lagoons, earthworm droppings, marine coastal sediments and pond water. *R. palustris* exhibits a surprising versatility and can switch between any of the four different metabolic states: photoautotrophic, photoheterotrophic, chemoautotrophic and chemoheterotrophic. This versatile metabolic nature has received significant attention in recent years due to the potential implications as bacterium suitable for biotechnological and industrial applications: industrial waste, inorganic and organic compounds including green plant-derived, pollutants and aromatic compounds, can be degraded by *R. palustris* and converted into either biomass or biofuel (Larimer et al., 2004; Oda, Star, Huisman, Gottschal, & Forney, 2003).

The versatile nature of *R. palustris* and its ability to adapt to various environments prompted us to focus the attention on its membrane characteristics. The ability of hopanoids, bacterial surrogated of eukaryotic sterols, in maintaining membrane integrity and assure membrane permeability has been demonstrated (Welander et al., 2009). Furthermore, it is well recognized that bacterial surfaces are highly decorated with saccharidic motifs responsible for mediating cell–environment interaction (Raetz & Whitfield, 2002; Silipo, De Castro, Lanzetta, Parrilli, & Molinaro, 2010; Silipo, Molinaro et al., 2010). The peculiarities of *R. palustris* and the role likely played by cell wall components, conveyed our efforts in defining the structure of membrane glycoconjugates. In particular, we focused our attention on lipopolysaccharides (LPSs), the major and vital components of the bacterial outer membrane (Raetz & Whitfield, 2002). LPSs have common structural motifs comprising a hydrophilic heteropolysaccharide (formed by a core oligosaccharide and an O-specific polysaccharide or O-chain) covalently linked to the lipophilic moiety named lipid A. The O-specific chain is the structurally variable LPS portion and is characterized by a high specificity within a species. Functionally, since they are

* Corresponding author. Tel.: +39 081 674404; fax: +39 081 674393.
E-mail address: silipo@unina.it (A. Silipo).

http://dx.doi.org/10.1016/j.carbpol.2014.08.037
0144-8617/

among the most exposed cell envelope components, LPS play a central role in the mechanisms of bacterial invasion and adaptation participating in host-bacterium events like adhesion, colonization, virulence, symbiosis and interaction with host physiology, and are therefore fundamental for bacterial growth and viability. The O-chain is the LPS portion more exposed to the selective pressures of the outer environment and to modification induced by external stimuli; among its various roles, the most important appears to be protective, acting as a defensive barrier.

In this work, we have investigated the structural and conformational features of the O-chain region of LPS isolated from *R. palustris* strain BisA53. We showed that this strain produces a polymer based on a trisaccharide repeating unit characterized by D-rhamnose, 3-deoxy-D-*lyxo*-2-heptulosaric acid (Dha), and a novel C-branched monosaccharide, the 4-amino-4,6-dideoxy-3-*C*-methyl-2-*O*-methyl-α-L-glucopyranose. This latter, to the best of our knowledge, has been found for the first time in Nature, thus, its absolute configuration has been determined by a combination of 2D NMR spectroscopy and molecular mechanics and dynamics (Lipkind, Shashkov, Mamian, & Kochetkov, 1988; Jimenez-Barbero et al., 2002; Silipo, De Castro et al., 2010; Silipo, Molinaro et al., 2010). Moreover, a conformational study was executed on the whole polymer with the aim of evaluating its spatial arrangements by the same combined approach. An accurate investigation of the structural and conformational features of the O-chain produced by this bacterial strain when cultivated *in vitro* is a first useful step to investigate the (bio)chemical adaptation of *R. palustris* BisA53 external surface to different environments.

2. Material and methods

2.1. Bacterial strain and growth condition

The *R. palustris* BisA53 strain was grown anaerobically at 28 C in Hutner medium (Clayton, 1963) in closed flask of 5 l exposed to continuous white light. After 5 days, the cells of 40 l of culture were harvested by centrifugation and freeze-dried.

2.2. Extraction, purification, SDS-PAGE analysis, LPS isolation

Dried cells were extracted by the phenol/water method (Westphal & Jahn, 1965). After extensive dialyses against distilled water, the extracted phases were subjected to enzymatic digestions in order to remove nucleic acids and proteins contaminants. Then, both water and phenol fractions were analyzed through SDS-PAGE 13.5% and LPS fraction was exclusively found in water phase as suggested by the presence of the typical ladder in its migration pattern in the gel (data not shown).

2.3. Production of PS1 and PS2 polysaccharides

The O-chain moiety (**PS1**) was isolated performing a mild acid hydrolysis. Purified LPS was dissolved in acetate buffer (pH = 4.4) and the hydrolysis was run for 3 h at 100 °C. After lipid A removal by centrifugation, the water-soluble product was further purified on gel filtration chromatography on a Sephacryl S-100 column. **PS1** polysaccharide was then *O*-deacylated with anhydrous hydrazine, 37 °C, 1 h to give **PS2** product.

2.4. Chemical analysis

Determination of sugars residues and of their absolute configuration through GC–MS analysis, were all carried out as described (Leontein & Lönngren, 1978). Monosaccharides were identified as acetylated *O*-methyl glycosides derivatives. After methanolysis (2 M HCl/MeOH, 85 °C, 18 h) and acetylation with acetic anhydride in pyridine (85 °C, 30 min) the sample was analyzed by GC-MS. The absolute configuration of sugar residues has been determined by GC–MS analysis of the acetylated *O*-(+)-2-octyl glycosides derivatives and comparison with authentic standards. Linkage analysis was carried out by methylation of the complete O-chain region as described (Hakomori, 1964; briefly, the sample was methylated with iodomethane, hydrolyzed with 2 M trifluoroacetic acid (100 °C, 2 h), carbonyl-reduced with $NaBD_4$, acetylated with acetic anhydride and pyridine, and analyzed by GC–MS.

2.5. NMR analysis

For structural assignments, 1D and 2D ^{1}H NMR spectra were recorded in D_2O at pD 7, at 298 K on Bruker 600 DRX equipped with a cryo probe. Spectra were calibrated with internal acetone [δ_H 2.225, δ_C 31.45]. ROESY and NOESY experiments were recorded using data sets ($t_1 \times t_2$) of 4096 × 256 points with mixing times between 100 ms and 300 ms. Double quantum-filtered phase-sensitive COSY experiments were performed using data sets of 4096 × 256 points. TOCSY experiments were performed with spinlock times of 100 ms, using data sets ($t_1 \times t_2$) of 4096 × 256 points. In all homonuclear experiments the data matrix was zero-filled in both dimensions to give a matrix of 4 K × 2 K points and was resolution enhanced in both dimensions by a cosine-bell function before Fourier transformation. Coupling constants were determined by 2D phase sensitive DQF-COSY (Piantini, Sørensen & Ernst, 1982; Rance et al., 1983). HSQC and HMBC experiments were measured in the ^{1}H-detected mode via single quantum coherence with proton decoupling in the ^{13}C domain, using data sets of 2048 × 256 points. Experiments were carried out in the phase-sensitive mode (States, Haberkorn & Ruben, 1982). A 60 ms delay was used for the evolution of long-range connectivities in the HMBC experiment. In all heteronuclear experiments the data matrix was extended to 2048 × 1024 points using forward linear prediction extrapolation.

2.6. Conformational studies

Molecular mechanics calculations were performed using the MM3* force field as included in MacroModel 8.0. A dielectric constant of 80 was used. For each disaccharide structure, both Φ and Ψ were varied incrementally using a grid step of 18°, each (Φ, Ψ) point of the map was optimized using 2000 P.R. conjugate gradients. The molecular dynamic simulations were run by using the MM3* force field; bulk water solvation was simulated by using MacroModel generalized Born GB/SA continuum solvent model. All simulations were performed at 300 K, structures were initially subjected to an equilibration time of 300 ps, then a 5000 ps molecular dynamic simulation was performed with a dynamic time-step of 1.5 fs, a bath constant *t* of 0.2 ps and the SHAKE protocol to the hydrogen bonds. Trajectory coordinates were sampled every 2 ps, and a total of 5000 structures were collected for every simulation (Asensio et al., 2000; Ieranò et al., 2009). Ensemble average-interproton distances were calculated using the NOEPROM program (Bernardi et al., 2002) by applying the isolated spin pair approximation as described (Asensio & Jimenez-Barbero, 1995). Coordinate extractions were performed with the program SuperMap, supplied with the NOEPROM package, and data visualized with ORIGIN software. Solvent-accessible surfaces were calculated with the surface utility of Macromodel and with molecular surface displays of ViewerPro Version 4.2.

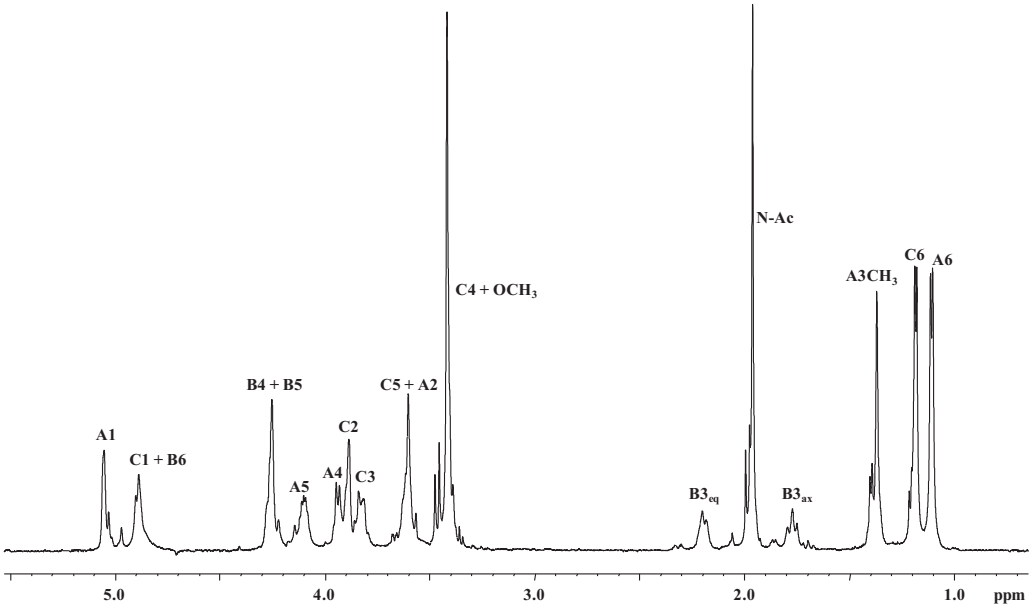

Fig. 1. ^{1}H NMR spectrum of **PS2** product. Signals are as attributed in Table 1.

3. Results and discussion

3.1. LPS extraction and chemical analysis

Dried cells were extracted by hot phenol/water protocol (Westphal & Jahn, 1965). The SDS-PAGE analysis showed that LPS was of smooth type, according to the presence of high molecular weight species in the upper part of the gel (data not shown).

Chemical analysis of LPS fraction showed the presence of D-rhamnose, 3-deoxy-D-*lyxo*-2-heptulosaric acid (Dha) and of a 4-amino-4,6-dideoxy-3-*C*-methyl-2-*O*-methyl-Hex*p* (Fig. S1). The absolute configuration of rhamnose and DHA was determined by GLC of the acetylated (*S*)-2-octyl glycosides and comparison with authentic standard whereas for the new monosaccharide residue this was established by NMR and MD approach (as described below). Methylation analysis showed the presence of 3-substituted D-Rha*p*; 5-substituted D-Dha*p*; 3-substituted 4-amino-4,6-dideoxy-3-*C*-methyl-2-*O*-methyl-Hex*p*.

3.2. NMR analysis

In order to isolate the O-chain, a mild acid hydrolysis was performed and the water soluble polysaccharide was purified by gel-permeation chromatography (**PS1**) and underwent NMR analysis; however, since **PS1** gave evidence of non stoichiometric *O*-acylation (Figs. S2–S4), we decided to simplify the NMR analyses by a *O*-deacylation performed with anhydrous hydrazine; the obtained *O*-deacylated polysaccharide (**PS2**) was further purified and characterized by full 2D NMR analysis.

The ^{1}H NMR spectrum of the **PS2** product is shown in Fig. 1. A combination of homo- and heteronuclear 2D NMR experiment (DQF-COSY, TOCSY, ROESY, NOESY, ^{1}H–^{13}C HSQC, ^{1}H–^{13}C HMBC) was executed to assign all the spin systems and to define the saccharidic sequence. The anomeric configuration of each monosaccharide unit was assigned on the basis of $^{3}J_{H\text{-}1,H\text{-}2}$ and $^{1}J_{CH}$ coupling constants, whereas the values of the vicinal $^{3}J_{H,H}$ ring coupling constants allowed the identification of the relative configuration of each sugar residue.

Residue **C** (Table 1 and Fig. 1) was recognized as α-rhamnose as indicated by the scalar correlations, in the TOCSY spectrum, of the ring protons with C-6 methyl signal (Fig. 2). The *manno* configuration was established by $^{3}J_{H\text{-}1,H\text{-}2}$ and $^{3}J_{H\text{-}2,H\text{-}3}$ (both below 2 Hz), $^{3}J_{3,4}$ (3 Hz) and $^{3}J_{H\text{-}4,H\text{-}5}$ (9 Hz), the α-anomeric configuration was assigned by the $^{1}J_{CH}$ coupling constant value of 175.9.

Because of the absence of the anomeric proton signal, spin system of Dha **B** was assigned starting from the diastereotopic H-3 methylene protons (Table 1 and Figs. 1 and 2), resonating in a shielded region at 1.78 and 2.20 ppm (H-3ax and H-3eq,

Table 1
^{1}H and ^{13}C NMR chemical shifts (ppm) of **PS2** measured at pD7. Due to the presence of two carboxyl groups in residue **B**, chemical shifts of this latter might slightly change at different pDs.

[→3)-**C**-(1→3)-**A**-(1→5)-**B**-(2→]$_n$							
Unit	1	2	3	4	5	6	7
A	5.04	3.60	–	3.93	4.09	1.10	
3-α-Sug	96.9	80.3	77.6	54.9	65.5	16.9	
		O—CH_3 3.41/58.3	CH_3 1.37/16.9	Acetyl C=O 173.64, CH_3 1.97/22.0			
	$^{1}J_{CH}$ 173.9 Hz	$^{3}J_{H\text{-}1,H\text{-}2}$ 2 Hz		$^{3}J_{H\text{-}4,H\text{-}5}$ 10.7 Hz			
B	–	–	2.2/1.78	4.26	4.25	4.88	–
5-α-DHA	177.3	99.0	34.9	65.0	75.9	73.9	175.8
			$^{3}J_{H\text{-}3ax,H\text{-}4}$ 12.7 Hz; $^{3}J_{H\text{-}3aeq,H\text{-}4}$ 1 Hz		$^{3}J_{H\text{-}5,H\text{-}6}$ < 1 Hz		
C	4.80	3.89	3.82	3.40	3.61	1.18	
3-α-Rha	93.1	68.6	72.5	70.6	68.9	16.9	
	$^{1}J_{CH}$ 175.9 Hz						

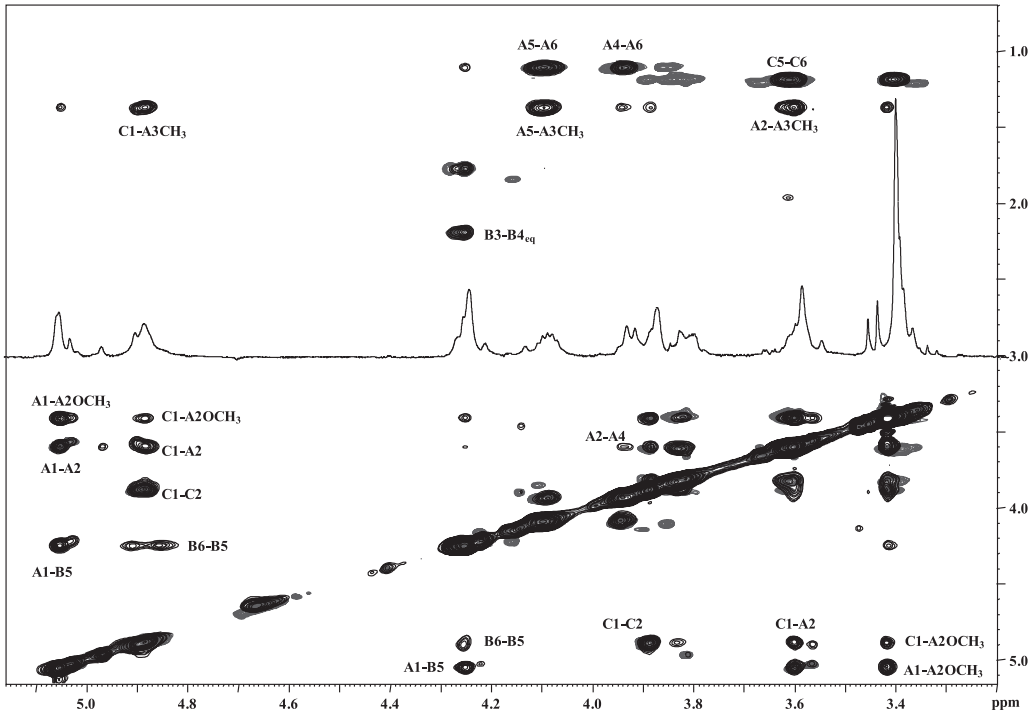

Fig. 2. ROESY (black) and TOCSY (gray) spectra related to **PS2** product. The main *inter*-residual correlations used to assign, together with the HMBC spectrum, the sugar backbone, are indicated; key *intra*-residual NOE correlations are also indicated. Letters are as reported in Table 1.

respectively). The *lyxo*-configuration of the Dha was deduced from the coupling constants $^{3}J_{H3ax,H4}$ of 12.7 Hz, indicative of the axial position of H-4, and of $^{3}J_{H5,H6} < 1$ Hz, corresponding to an equatorial disposition of H-5 in a $^{5}C_{2}$ chair conformation. The α-anomeric configuration of Dha was assigned on the basis of previously published data (Birnbaum, Roy, Brisson, & Jennings, 1987; Vinogradov et al., 1997).

Spin system **A** (Table 1) was identified as a 4-amino-4,6-dideoxy-3-*C*-methyl-2-*O*-methyl-α-glucose (3-*C*-methyl-2-*O*-methyl-4-amino-α-quinovose (further on abbreviated as 3-methyl-2-*O*-methyl-Qui4N). The α-anomeric configuration of **A** was supported by $^{3}J_{H-1,H-2}$ and $^{1}J_{C,H}$ coupling constant values of 2 Hz and 173.9 Hz, respectively (Table 1). The 2-*O*-methyl group was univocally located at C-2 **A** on the basis of the downfield shift of C-2 **A** (80.3 ppm, Table 1), by the long range correlations present in the HMBC spectrum of C-2 **A** with the proton signals of methoxy group and confirmed by the NOE contact of this latter with H-2 **A**. The anomeric proton signal of **A** at 5.04 ppm correlated exclusively with H-2; a second spin system was present, involving scalarly correlated proton signals from position 4 to position 6. The $^{3}J_{H-4,H-5}$ coupling constant value of 10.7 Hz was used to establish the relative *axial* configuration of both H-4 and H-5 protons (Table 1, Figs. 2 and 3); the scalar correlation of both H-4 and H-5 with a downfield methyl signal were indicative of the nature of 6-deoxysugar of **A**.

Furthermore, the HSQC spectrum (Fig. 3) showed a correlation of H-4 **A** with a nitrogen bearing carbon signal at 54.9 ppm that, together with the down-field shift of H-4 proton resonance, was diagnostic of *N*-acyl group at this position. In fact, the presence of the amino group was also confirmed by the long range correlation, in the HMBC spectrum, of H-4 **A** with the carbonyl carbon of the acetyl group and of this latter with a methyl group. The long range correlations in the HMBC spectrum (Fig. 3) were useful to completely identify residue **A**. In particular, the long range correlations of a quaternary carbon with H-1, H-2 and H-4 **A** were indicative of the presence of a quaternary carbon at position C-3 of residue **A**. The substitution of C-3 **A** by a methyl group was identified by its long range correlations with the singlet methyl at 1.37/16.9 ppm (Fig. 3).

By NOE correlations found in the NOESY spectrum, the relative configuration of monosaccharide **A** was also established. Actually, the axial orientation of CH_3 on C-3 was endorsed by the *intra*-residual NOE with the *syn*-axial proton H-5 at 4.09 ppm (Fig. 2); likewise, the *intra*-residue NOE contacts between H-2 and H-4 indicated their *syn*-diaxial orientation. To summarize, the $^{3}J_{H,H}$ ring coupling constant values, NOE and HMBC correlations suggested a *gluco* configuration for residue **A**, a 3-*C*-methyl-4-amino-α-quinovose carrying a methyl group at position O-2.

The downfield shift of carbon resonances identified the glycosylated positions: O-3 of residues **A** and **C** and O-5 of **B**, in full agreement with the methylation analysis. The sequence of this repeating unit was defined by the long-range scalar correlations found in the HMBC spectrum and the *inter*-residual NOE contacts. Residue **A** was glycosylated at O-3 by α-rhamnose **C**, as suggested by the long range scalar correlation H-1 **C**/C-3 **A** and the NOE contact of H-2 **A** with H-1 **C** (Figs. 2 and 3). Residue **C** was in turn glycosylated at its O-3 by **B** residue, as attested by the long range contact of **B**-2 with **C**-3; eventually, residue **B** was substituted at its C-5 by residue **A** as attested by the NOE between H-1 **A** and H-5 **B** (Fig. 2) and by the corresponding long range contacts. Thus, all data were in agreement with the primary structure reported below (Fig. 4):

3.3. Determination of the absolute configuration of *A* residue and molecular mechanics and dynamic simulations

In order to determine the absolute configuration of the 3-*C*-methyl-2-*O*-methyl-Qui4N (residue **A**), we have used a protocol based on NOE data and computational approach (Lipkind et al., 1988; Jimenez-Barbero et al., 2002; Silipo, De Castro et al., 2010; Silipo, Molinaro et al., 2010). Lipkind et al. demonstrated that main structural factors determining the preferred conformation in disaccharides, and therefore the corresponding NOEs, are the configuration of the glycosidic linkage, the nature of the sugar, the

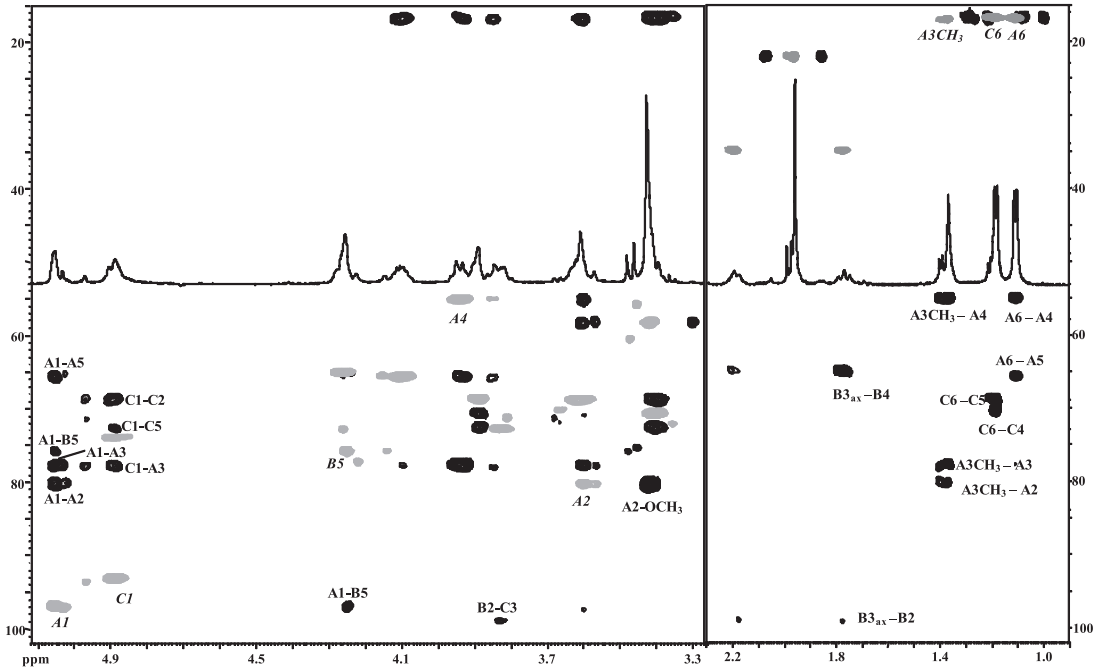

Fig. 3. HSQC (gray) and HMBC (black) spectra of **PS2** product; the key *inter*-residual and *intra*-residual long range correlations are indicated; letters are as referred in Table 1.

position of glycosylation and the absolute configuration of the constituent residues. Taking into account this above, and given that the absolute configuration of the other two residues **B** and **C** was known, we measured and compared the NOE-derived key *inter*-proton distances with those predicted for models taking in account the two possible absolute configurations of residue **A** (L and D).

The first step was the building of the potential energy surfaces for each disaccharide connected by a glycosidic linkage; Φ represents the torsion angle about H1-C1-O-CX' whereas Ψ about C1-O-CX'-H'; five distinct disaccharide entities were constructed (Fig. 5a) considering the above determined repeating unit: [→3)-**C**-(1→3)-**A**-(1→5)-**B**-(2→]$_n$ and the two possible absolute configurations of residue **A**, drawn with both D and L configuration (**A$_L$** and **A$_D$**) and subjected to extensive calculations using MM3* force field to build the potential energy surfaces for both disaccharides whose relative orientation is defined by Φ and Ψ torsion angles around the glycosidic linkage. The resulting adiabatic energy maps indicating global minima are reported in Fig. 5a.

C **A** **B**

[→3)-α-D-Rha-(1→3)-α-Sug-(1→5)-α-D-Dha-(2→]$_n$

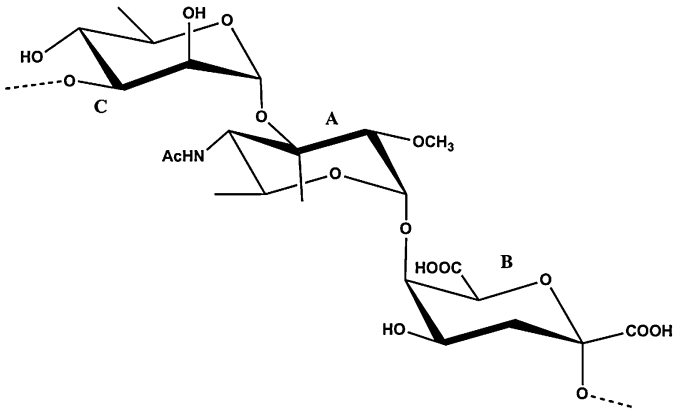

Fig. 4. Structure of the O-polysaccharide from *R. palustris* BisA53.

Molecular mechanic calculations furnished an estimation of the conformational regions energetically accessible and predicted the existence of slightly different minima for the glycosidic linkages involving **A** residue: the global minimum was located at Φ/Ψ 17/24 for **A1$_L$** → **B5**, and at Φ/Ψ 55/35 for **A1$_D$** → **B5** (Fig. 5a); as the glycoside linkage involving **C** and **A** residues, in **C1** → **A3$_L$** the global minimum was located at Φ/Ψ −46/−42 while in **C1** → **A3$_D$** two energetically comparable minima were present, located at −38/78 and −45/−38. Starting subsequently, two oligomers containing two and four repeating units and differing for the absolute configuration of **A** residue were built from the minima of the energy maps and the conformational behavior was studied by using molecular dynamic simulation:

$$\mathbf{C_1 \rightarrow 3A_{L1} \rightarrow 5B_1 \rightarrow 3C_2 \rightarrow 3A_{L2} \rightarrow 5B_2 \rightarrow 3C_3 \rightarrow 3A_{L3} \rightarrow 5B_3 \rightarrow 3C_3 \rightarrow 3A_{L3} \rightarrow 5B_3}$$

$$\mathbf{C_1 \rightarrow 3A_{D1} \rightarrow 5B_1 \rightarrow 3C_2 \rightarrow 3A_{D2} \rightarrow 5B_2 \rightarrow 3C_3 \rightarrow 3A_{D3} \rightarrow 5B_3 \rightarrow 3C_3 \rightarrow 3A_{D3} \rightarrow 5B_3}$$

The initial structures were extensively minimized and trajectory coordinates were sampled every ps; 5000 simulations were performed in GB/SA water solvation model as implemented in MacroModel (MMOD); Φ/Ψ scatter plots of the central glycosidic linkages are shown in Fig. S5. A first analysis of MD results showed that torsion angles remained in the broad low energy regions previously predicted by the MM calculation, although **C** → **3A$_D$** torsion almost selected the minimum around −45/−38 (see Fig. 5a and Fig. S7). The computational models obtained from the MD were then compared to the experimental results. Ensemble average *inter*-proton distances for each saccharide entity were extracted from dynamic simulations and translated into predicted NOEs by a full-matrix relaxation approach. The corresponding average distances obtained for the simulation from $\langle r^{-6} \rangle$ values and predicted for both the hexasaccharides built with residue **A** in D and L configuration

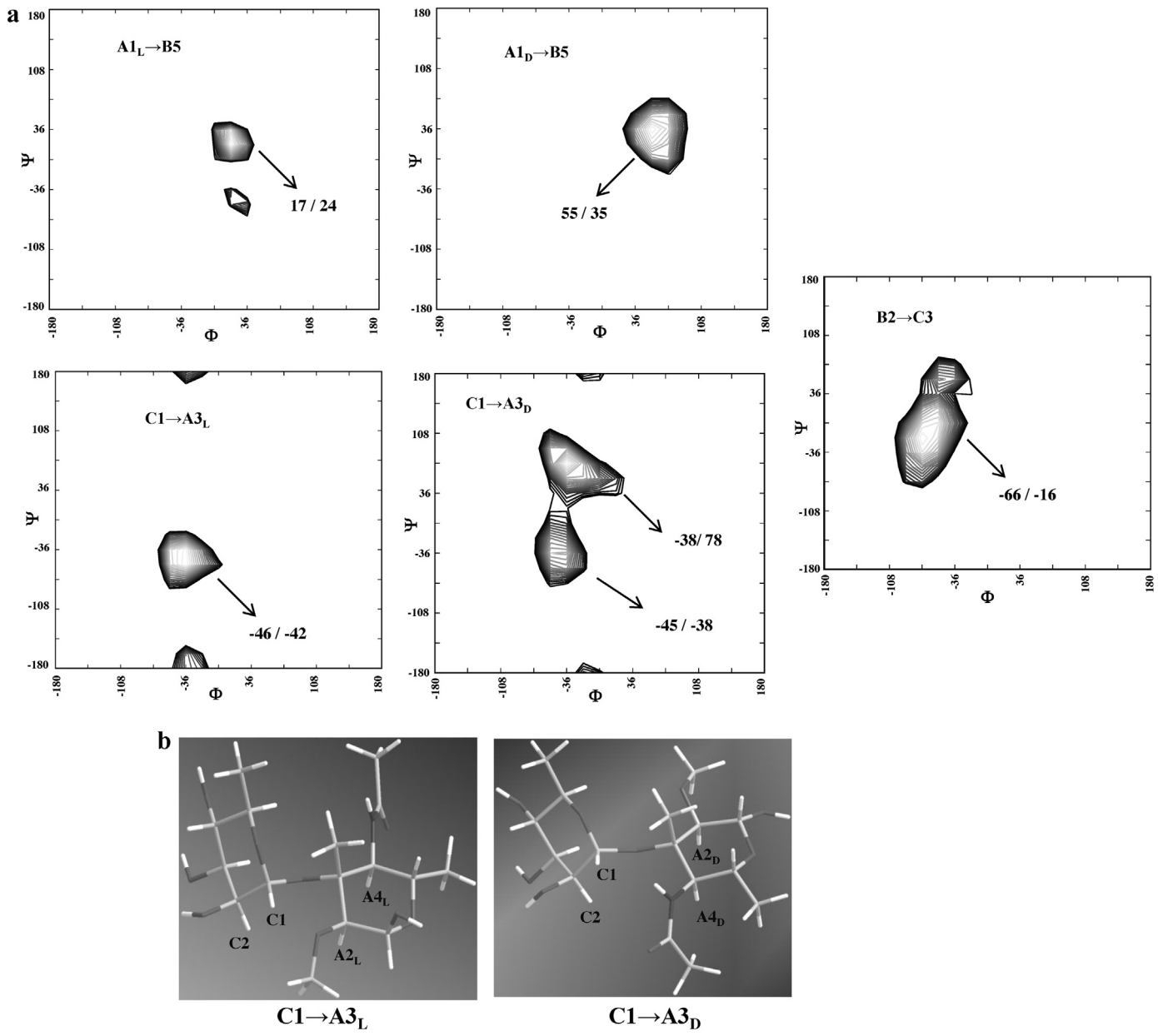

Fig. 5. (a) Relaxed energy maps for the disaccharide fragments composing the O-polysaccharide from *R. palustris* BisA53; the two maps for **A1** → **B5** linkage differ in the absolute configuration of **A** residue. The positions of global and major local minima in the maps are indicated. (b) View of representative structures of **A1** → **B5** disaccharides differing in the absolute configuration of **A**; key protons for the definition of the absolute configuration of **A** are indicated (see text); color version reported in Fig. S5.

were compared to those collected experimentally (Table 2). A comparison of the simulated and measured distances allowed us to evaluate the absolute stereochemistry of residues **A**, that resulted to be L for which case an excellent agreement was found between calculated and experimental data. In detail, the key NOEs and derived distances considered for the definition of the absolute configuration of **A** were those of H-1 **C** with H-2 **A** (strong) and of H-1 **C** with H-2 **A** (medium), only predictable with L configuration of **A** (see Table 2, Figs. 2, 5a and b and Fig. S5), in which the H-1 and H-2 of the α-rhamnose **C** point toward and H-2 **A** and far from H-4 **A** (the side of the sugar ring of **A** residue containing H-2 and far from the side containing H-4); as a further confirmation, a mild-strong NOE contact also with **A2**-OCH_3 was present in the NOESY spectrum (Figs. 2 and 5b and Fig. S5). In case of a D configuration, NOE effects of H-1 and H-2 **C** with H-4 **A** were expected (Table 2, Figs. 2 and 5b) and, conversely, the NOE of H-1/H-2 **C** with H-2 **A** would have been absent (Table 2; Fig. 5b).

The effect of the different relative orientation of **A** and **C** rings could be in turn translated into a different three-dimensional arrangement of the two above oligomers (Figs. 6a and b and Fig. S6), built with four repeating units and differing for the absolute configuration of **A**. The shape of the dodecasaccharide, reported in Fig. 6a and b and Fig. S6, showed the differences in the conformational and spatial arrangement. The oligomer with **A** residue in D configuration gave rise to a more compact and pace structure while the oligomer with **A** in L configuration assumed a more extended conformation with a helicoidal disposition.

3.4. NMR analysis of the fully acylated sample PS1

In order to complete the structure of the polysaccharide produced by *R. palustris* strain BisA53, we also have assigned the fully acylated polysaccharide **PS1**. The NMR data (Figs. S2–S4) gave evidence of acylation shift; analysis of homo- and heteronuclear

Table 2
Experimental (from NOESY experiments) and calculated (from MD calculations) *inter*-proton distances for oligomer built with two and four repeating units. The experimental values were obtained as described in the experimental part by applying the isolated spin pair approximation.

$C_1 \rightarrow 3A_{L1} \rightarrow 5B_1 \rightarrow 3C_2 \rightarrow 3A_{L2} \rightarrow 5B_2$ and $C_1 \rightarrow 3A_{D1} \rightarrow 5B_1 \rightarrow 3C_2 \rightarrow 3A_{D2} \rightarrow 5B_2$

	Experimental 100 ms	Experimental 200 ms	Observed NOE	Hexasaccharide - calculated D		Hexasaccharide-calculated L	
A1-B5	2.79	2.85	Strong	2.85 ± 0.29	2.80 ± 0.27	2.74 ± 0.26	2.75 ± 0.27
C1-A2	2.89	2.99	Strong	4.45 ± 0.12	4.20 ± 0.44	3.16 ± 0.37	3.16 ± 0.27
C2-A2	3.40	3.35	Medium	4.49 ± 0.25	4.60 ± 0.35	3.57 ± 0.41	3.53 ± 0.28
C1-A4	–	–	Absent	3.43 ± 0.24	3.64 ± 0.49	4.26 ± 0.44	4.37 ± 0.15
C2-A4	–	–	Absent	3.79 ± 0.25	4.00 ± 0.30	4.31 ± 0.31	4.35 ± 0.24

$C_1 \rightarrow 3A_{L1} \rightarrow 5B_1 \rightarrow 3C_2 \rightarrow 3A_{L2} \rightarrow 5B_2 \rightarrow 3C_3 \rightarrow 3A_{L3} \rightarrow 5B_3 \rightarrow 3C_3 \rightarrow 3A_{L3} \rightarrow 5B_3$
$C_1 \rightarrow 3A_{D1} \rightarrow 5B_1 \rightarrow 3C_2 \rightarrow 3A_{D2} \rightarrow 5B_2 \rightarrow 3C_3 \rightarrow 3A_{D3} \rightarrow 5B_3 \rightarrow 3C_3 \rightarrow 3A_{D3} \rightarrow 5B_3$

	Dodecasaccharide - calculated L					Dodecasaccharide - calculated D			
A1-B5	2.75 ± 0.27	2.75 ± 0.26	2.75 ± 0.26	2.75 ± 0.25	A1-B5	2.84 ± 0.27	2.83 ± 0.27	2.84 ± 0.27	2.82 ± 0.27
C1-A2	3.16 ± 0.26	3.16 ± 0.25	3.17 ± 0.24	3.15 ± 0.26	C1-A2	4.37 ± 0.12	4.37 ± 0.15	4.38 ± 0.22	4.00 ± 0.44
C1-A4	4.37 ± 0.14	4.37 ± 0.14	4.37 ± 0.13	4.3 ± 0.13	C1-A4	3.38 ± 0.25	3.37 ± 0.28	3.38 ± 0.25	3.76 ± 0.44
C2-A2	3.50 ± 0.28	3.53 ± 0.27	3.54 ± 0.25	3.53 ± 0.27	C2-A2	4.50 ± 0.28	4.49 ± 0.28	4.50 ± 0.27	4.69 ± 0.28
C2-A4	4.32 ± 0.24	4.35 ± 0.22	4.36 ± 0.22	4.35 ± 0.23	C2-A4	3.84 ± 0.22	3.81 ± 0.24	3.83 ± 0.27	4.00 ± 0.35

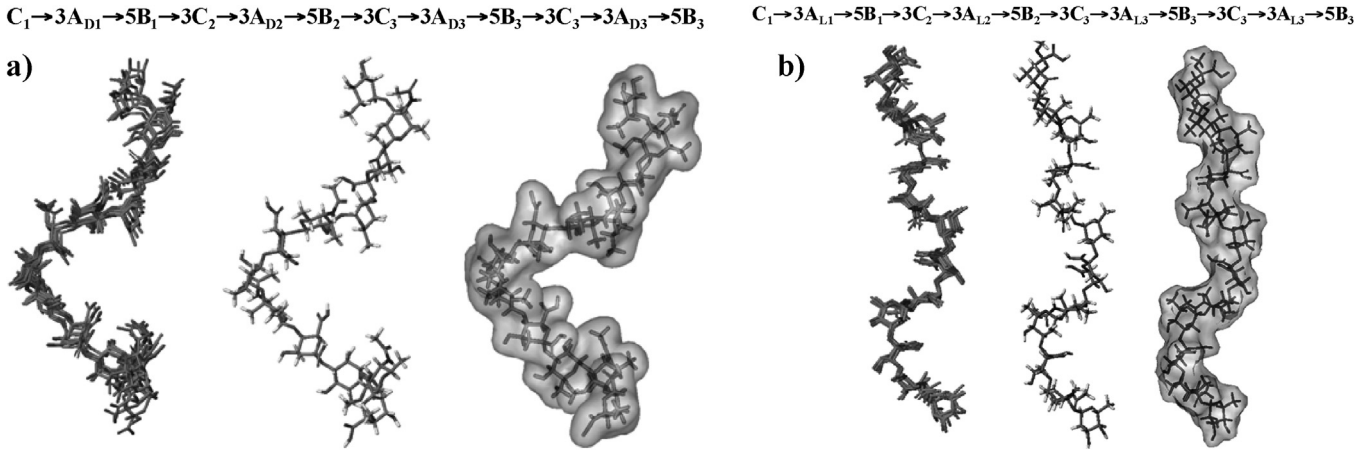

Fig. 6. View of representative structures and Connelly surface of **PS2** species built with four repeating units; the two dodecasaccarides **[$C_1 \rightarrow 3A_{D1} \rightarrow 5B_1$]$_4$** (a) and **[$C_1 \rightarrow 3A_{L1} \rightarrow 5B_1$]$_4$** (b) differ for the absolute configuration of **A** residue; color version reported in Fig. S6.

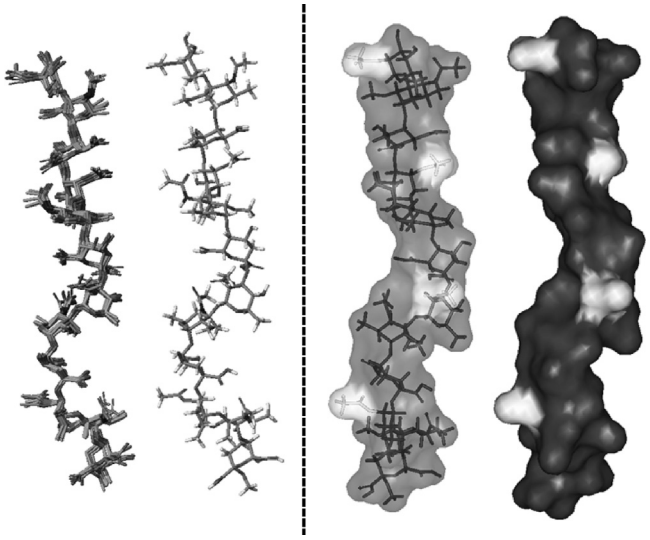

Fig. 7. View of representative structures and Connelly surface of **PS1**; the preferential disposition of the acetyl groups of the rhamnose units is highlighted (light gray).

NMR experiments allowed to locate as responsible an acetyl group at position 2 of the α-rhamnose **C**. A thorough inspection of the spectra also allowed identifying signals belonging to the non-acetylated polysaccharide; actually, the integration of the isolated signals allowed to establish that the major acetylated polysaccharide was present at 60–70% of abundance.

The fully acetylated polymer underwent an MD simulation; a dodecasaccharide fragment composed of four repeating units was built from the global minima of the energy maps and the conformational behavior was studied by using molecular dynamic simulation. MD results showed that trajectories remained in the broad low energy regions previously predicted by the MM calculation (not shown) and adopted a behavior quite similar to the non-acetylated compound. Actually, the surfaces of the two dodecasaccharides were built according to the Connelly method (Figs. 6b and 7 and Fig. S8) to gain additional information regarding the overall shape of these species. Both species adopted a helicoidal shape and, as evident from Fig. 7, the acetylated polymer regularly exposed the acetyl group outside with the acetyl groups pointed outward the saccharide chain.

4. Conclusions

We here defined the full structure and conformational behavior of the O-chain polysaccharide isolated from *R. palustris* strain

BisA53. The O-chain consisted of a novel trisaccharide repeating unit made up of rhamnose, non stoichiometrically acetylated at O-2, and Dha, both D configured, and of a novel monosaccharide, a derivative of 4-amino-L-quinovose, branched by a methyl group at carbon 3 and carrying a methoxy group at O-2; its absolute configuration was defined by using an NMR-based molecular mechanics approach.

The combined NOE-based molecular dynamics approach allowed a satisfactory description of both 3D structures; a complete study of the O-chain highlighted a significant level of hydrophobicity since it was constituted by three deoxy-sugars variously decorated by acetyl and methyl groups, acting as shield of hydroxy and amino groups and thus further increasing the polysaccharide hydrophobic character.

The bacterial genus *Rhodopseudomonas* comprises photosynthetic bacteria widely distributed in aquatic sediments; the genome sequence revealed a surprisingly rich metabolically versatility, that explains its ability to live in a heterogeneous environments and corroborates its potential use in biotechnological applications. *Rhodopseudomonas* strains modulate photosynthesis according to light, degrade aromatic agricultural and industrial pollutants, catalyze hydrogen gas production, carbon dioxide sequestration, and biomass turnover (Oda et al., 2008).

LPS O-antigen modifications generally seem to play an important role at several stages of bacterial adaptation to external environments and might increase the binding and adhesion capacity of the bacterial strains, including the colonization (adherence) step. This is usually attained by bacterial cells through chemical modifications on pre-synthesised repeating units; among these, acetylation is thought to increase viscosity and emulsifying properties (Lerouge & Vanderleyden, 2001). These carbohydrate based polymers are of interest for the potential biotechnological exploitation as, for example, emulsifying or suspending agents, in the field of food, cosmetic, textile industries, for the capacity of modifying flow properties of water, as metal ion sequestrating agents, in the pharmaceutical industries (Larimer et al., 2004; Silipo, De Castro et al., 2010; Silipo, Molinaro et al., 2010).

Acknowledgements

The 600 MHz cryoprobe NMR facilities were provided by the spectrometer of the Centro Regionale di Competenza in Biotecnologie Industriali BioTekNet. This study was supported (to A.M.) by PRIN MIUR 2011 L9SH3K (Italian Ministry for University and Research).

Appendix A. Supplementary data

Supplementary data associated with this article can be found, in the online version, at http://dx.doi.org/10.1016/j.carbpol.2014.08.037.

References

Asensio, J. L., & Jimenez-Barbero, J. (1995). The use of the AMBER force field in conformational analysis of carbohydrate molecules: Determination of the solution conformation of methyl alpha-lactoside by NMR spectroscopy, assisted by molecular mechanics and dynamics calculations. *Biopolymers*, *35*, 55–75.

Asensio, J. L., Cañada, F. J., Cheng, X., Khan, N., Mootoo, D. R., & Jiménez-Barbero, J. (2000). Conformational differences between O- and C-glycosides: The alpha-O-man-(1-1)-beta-Gal/alpha-C-Man-(1-1)-beta-Gal case - a decisive demonstration of the importance of the exo-anomeric effect on the conformation of glycosides. *Chemistry - A European Journal*, *6*, 1035–1041.

Bernardi, A., Potenza, D., Capelli, A. M., Garcia-Herrero, A., Canada, F. J., & Jimenez-Barbero, J. (2002). Second-generation mimics of ganglioside GM1 oligosaccharide: A three-dimensional view of their interactions with bacterial enterotoxins by NMR and computational methods. *Chemistry - A European Journal*, *8*, 4598–4612.

Birnbaum, G. I., Roy, R., Brisson, J. R., & Jennings, H. J. (1987). Conformations of ammonium 3-deoxy-D-manno-2-octulosonate (KDO) and methyl alpha- and beta-ketopyranosides of KDO: X-ray structure and ^{1}H NMR analyses. *Journal of Carbohydrate Chemistry*, *6*, 17–39.

Clayton, K. (1963). Toward the isolation of a photochemical reaction center in *Rhodopseudomonas spheroides*. *Biochimica et Biophysica Acta*, *75*, 312–318.

Hakomori, S. (1964). A rapid permethylation of glycolipid, and polysaccharide catalyzed by methylsulfinyl carbanion in dimethyl sulfoxide. *The Journal of Biochemistry*, *55*, 205–208.

Ieranò, T., Silipo, A., Cescutti, P., Leone, M. R., Rizzo, R., Lanzetta, R., et al. (2009). Structural study and conformational behavior of the two different lipopolysaccharide O-antigens produced by the cystic fibrosis pathogen *Burkholderia multivorans*. *Chemistry - A European Journal*, *15*, 7156–7166.

Jimenez-Barbero, J., de Castro, C., Evidente, A., Molinaro, A., Parrilli, M., & Surico, G. (2002). Structural determination of the O-specific chain of the lipopolysaccharide from *Pseudomonas cichorii*. *European Journal of Organic Chemistry*, *2002*, 1770–1775.

Larimer, F. W., Chain, P., Hauser, L., Lamerdin, J., Malfatti, S., Do, L., et al. (2004). Complete genome sequence of the metabolically versatile photosynthetic bacterium *Rhodopseudomonas palustris*. *Nature Biotechnology*, *22*, 55–61.

Leontein, K., & Lönngren, J. (1978). *Methods in Carbohydrate Chemistry*, *62*, 359–362.

Lerouge, I., & Vanderleyden, J. (2001). O-Antigen structural variation: Mechanisms and possible roles in animal/plant-microbe interactions. *FEMS Microbiology Reviews*, *26*, 17–47.

Lipkind, G. M., Shashkov, A. S., Mamian, S. S., & Kochetkov, N. K. (1988). The nuclear overhauser effect and structural factors determining the conformations of disaccharide glycosides. *Carbohydrate Research*, *181*, 1–12.

Oda, Y., Larimer, F. W., Chain, P. S., Malfatti, S., Shin, M. V., Vergez, L. M., et al. (2008). Multiple genome sequences reveal adaptations of a phototrophic bacterium to sediment microenvironments. *Proceedings of the National Academy of Science*, *105*(47), 18543–18548.

Oda, Y., Star, B., Huisman, L. A., Gottschal, J. C., & Forney, L. J. (2003). Biogeography of the purple nonsulfur bacterium *Rhodopseudomonas palustris*. *Applied and Environmental Microbiology*, *69*(9), 5186–5191.

Piantini, U., Sørensen, O. W., & Ernst, R. R. (1982). Multiple quantum filters for elucidating NMR coupling networks J. *Journal of the American Chemical Society*, *104*, 6800–6801.

Raetz, C. R., & Whitfield, C. (2002). Lipopolysaccharide endotoxins. *Annual Review of Biochemistry*, *71*, 635–700.

Rance, M., Sørensen, O. W., Bodenhausen, G., Wagner, G., Ernst, R. R., & Wüthrich, K. (1983). Improved spectral resolution in COSY ^{1}H NMR spectra of proteins via double quantum filtering. *Biochemical and Biophysical Research Communications*, *117*, 479–485.

Silipo, A., De Castro, C., Lanzetta, R., Parrilli, M., & Molinaro, A. (2010). Lipopolysaccharides. In H. König, H. Claus, & A. Varma (Eds.), *Prokaryotic cell wall compounds – structure and biochemistry* (pp. 133–154). Heidelberg: Springer.

Silipo, A., Molinaro, A., Molteni, M., Rossetti, C., Parrilli, M., & Lanzetta, R. (2010). Full structural characterization of an extracellular polysaccharide produced by the freshwater cyanobacterium *Oscillatoria planktothrixFP1*. *European Journal of Organic Chemistry*, *2010*(29), 5594–5600.

States, D. J., Haberkorn, R. A., & Ruben, D. J. (1982). A two-dimensional nuclear overhauser experiment with pure absorption phase in four quadrants. *Journal of Magnetic Resonance*, *48*, 286–292.

Vinogradov, E. V., Müller-Loennies, S., Petersen, B. O., Meshkov, S., Thomas-Oates, J. E., Holst, O., et al. (1997). Structural investigation of the lipopolysaccharide from *Acinetobacter haemolyticus* strain NCTC 10305 (ATCC 17906 DNA group 4). *European Journal of Biochemistry*, *247*(1), 82–90.

Welander, P. V., Hunter, R. C., Zhang, L., Sessions, A. L., Summons, R. E., & Newman, D. K. (2009). Hopanoids play a role in membrane integrity and pH homeostasis in *Rhodopseudomonas palustris* TIE-1. *Journal of Bacteriology*, *191*(19), 6145–6156.

Westphal, O., & Jahn, K. (1965). Bacterial lipopolysaccharides: Extraction with phenol-water and further applications of the procedure. *Methods in Carbohydrate Chemistry*, *5*, 83–91.